1   **Title:** Directing Cholangiocyte Morphogenesis in Natural Biomaterial Scaffolds

2   **Authors:** Quinton Smith [1,2], Christopher Chen [3], Sangeeta Bhatia [1,2,4]

3   **Affiliations:** [1.] Howard Hughes Medical Institute, Chevy Chase, MD, 20815 USA.[2] David

4   H. Koch Institute for Integrative Cancer Research, Massachusetts Institute of Technology,

5   Cambridge, MA, 02142 USA. [3.] Department of Bioengineering, Boston University, Boston,

6   MA, 02215 USA. [4.] Department of Electrical Engineering and Computer Science,

7   Massachusetts Institute of Technology, Cambridge, MA, 02142 USA.

8

9   Corresponding Author: Sangeeta Bhatia

10

11   Address:

12   Koch Institute for Integrative Cancer Research

13   500 Main Street

14   Cambridge, MA 02142

15   Email: sbhatia@mit.edu

16

17   **ABSTRACT**

18

19   Patients with Alagille syndrome carry monogenic mutations in the Notch signaling

20   pathway and face complications such as jaundice and cholestasis. Given the presence

21   of intrahepatic ductopenia in these patients, Notch2 receptor signaling has been

22   implicated in driving normal biliary development and downstream branching

23   morphogenesis. As a result, *in vitro* model systems of liver epithelium are needed to

24   further mechanistic insight of biliary tissue assembly. Here, we systematically evaluate

25   primary human intrahepatic cholangiocytes as a candidate population for such a platform

26   and describe conditions that direct their branching morphogenesis. We find that

27   extracellular matrix presentation, coupled with mitogen stimulation, promotes biliary

28   branching in a Notch-dependent manner. These results demonstrate the utility of using

29   3D scaffolds for mechanistic investigation of cholangiocyte branching and provides a

30   gateway to integrate biliary architecture in additional *in vitro* models of liver tissue.

31

1

32

INTRODUCTION

34

35 The liver is the largest internal organ in the body and is responsible for performing over

36 500 different vital functions. These tasks include detoxifying drugs, storing nutrients, and

37 producing essential factors such as albumin, clotting proteins, and bile. At a microscopic

38 view, the liver organization consists of repeated hexagonal units termed hepatic lobules.

39 These lobules contain sheets of hepatocytes, flanked by six portal triads, which are

40 comprised of a network of portal veins, hepatic arteries, and intrahepatic bile ducts. In this

41 triad, the vasculature is responsible for the transport of oxygen, nutrients, and clotting

42 factors. The bile ducts, on the other hand, transport hepatocyte-secreted bile acid to the

43 small intestine. Efforts to study liver biology benefit from *in vitro* model systems that

44 recapitulate aspects of the tissue's native cellular composition and architecture. Existing

45 liver tissue engineering strategies have successfully incorporated human vascular

46 networks with primary hepatocytes *in vitro* [1–4]. However, cell sourcing remains a critical

47 bottleneck in our ability to study human intrahepatic biliary biology. Coupled with this

48 limitation, *in vitro* model systems of the biliary system primarily rely on rodent isolates [5],

49 immortalized cell lines [6,7], or adult/pluripotent stem cell-derivatives [8–14]. These

50 populations either do not display mature cholangiocyte marker expression or are limited

51 to forming a non-perfusable structure that lacks the branched architectures found in the

52 native liver.

53

54 Immortalized mouse hepatoblasts, with the capacity to differentiate into hepatocytes or

55 cholangiocytes, have been shown to form cystic ductal structures in extracellular matrix

56 (ECM) conditions that contain both laminin rich Matrigel and rat tail collagen I. This finding

57 contrasts with other epithelia, such as Madin-Darby canine kidney cells (MDCK), which

58 only require integrin engagement with collagen I motifs to polarize and expand as cysts

59 [15]. Notably, when mouse hepatoblasts are cultured in collagen I, they form branch-like

60 structures but are unable to polarize. Cystic efficiency in hepatoblast culture is dependent

61 on EGF and HGF stimulation, as well as metalloproteinase and TGFβ activity [16].

62 Consistent with these findings, immortalized progenitor-like small cholangiocytes derived

2

63   from mice cannot spread in collagen I matrices or form cystic structures in Matrigel but

64   require decellularized liver ECM to undergo branching morphogenesis [17]. To reduce the

65   complexity of xeno-derived matrices, synthetic hydrogel scaffolds can be engineered with

66   specific material properties such as stiffness, porosity, and adhesion densities, permitting

67   systematic decoupling of physicochemical cues necessary for tissue homeostasis and

68   morphogenesis. For example, immortalized normal rat intrahepatic cholangiocytes

69   (NRCs) [7] encapsulated in polyethylene glycol (PEG) pre-polymers that are functionalized

70   with fibronectin-derived RGD binding motifs can expand as cysts in a stiffness-dependent

71   manner. Soft (0.5 kilopascal) hydrogel matrices lead to frequent cyst formation, and

72   increased RGD concentrations encourage multi-lumenal features, but interconnected

73   branched epithelial structures could not be generated [18]. Furthermore, a variety of

74   approaches have been used to build perfusable biliary tubes, but the resulting channels

75   lack hierarchical structure, and are composed of rodent-derived cholangiocytes [19,20]. To

76   date, the vast majority of studies in this field have relied on rodent-derived cellular

77   material, and there are many examples in the liver tissue engineering field in which

78   findings obtained using mouse and rat cells do not correlate with the outcomes obtained

79   with human samples [21–25]. While the advent of immortalized human biliary cell lines can

80   help to reduce these variances, they present their own limitations, including a heavy

81   mutational burden that can lead to clonal variability from the original source and

82   transformation from the natural phenotype as in the case with hepatocytes [26] . Motivated

83   both by these advances and the remaining progress gaps, we sought to build upon

84   existing biliary platforms and investigated the potential to fabricate branched human

85   cholangiocyte networks, alongside cholangiocyte-lined channels.

86

87   To this end, we characterized commercially available adult-derived primary human

88   cholangiocytes and investigated their branching potential in 3D culture conditions. First,

89   we performed cellular profiling with biliary-specific surface markers and measured tissue-

90   specific enzymatic activity. After validating cholangiocyte-like identity of these isolates,

91   we conducted 3D culture experiments in natural biomaterial scaffolds containing varying

92   concentrations of mitogens relevant to liver development and regeneration. From these

93   studies, we found that growth factor cues and the extracellular matrix coax *in vitro* biliary

94   network assembly in a Notch signaling-dependent manner[1,27,28]. In addition, we

95   demonstrate that branching architectures of this human cholangiocyte-like population are

96   also supported in an engineered microfluidic platform that has been used previously as

97   an organ-on-chip model system[1,27,28]. This finding highlights the potential to harness

98   these primary human cells in this perfusable platform for future investigations of

99   cholangiocyte functionality including permeability, shear stress response, and transport

100   of bile fluid components such as cholic/chenodeoxycholic acids or xenobiotics.

101   Collectively, our combined approaches reinforce the role of EGF stimulation and Notch

102   signaling in biliary morphogenesis.

103

104

105   **RESULTS**

106

107   **Primary Intrahepatic Cholangiocytes Maintain Functional Marker Expression *In***

108   ***Vitro***

109

110   Sourcing human primary cholangiocytes remains a challenge due to their intrahepatic

111   localization, however pluripotent stem cell derivatives [10,29–31] or Lgr5+ enriched adult duct

112   progenitor populations acquired from biopsied samples [9], have been routinely used as

113   model systems to date. While these sources permit the expansion of cholangiocyte-like

114   cells as cystic organoids, their maintenance requires administration of a complex

115   chemical milieu that maintains a stem-like state and does not promote the self-assembly

116   of physiologically relevant branched architectures. Here, we appraised morphological

117   and functional features of commercially available, adult intrahepatic biliary epithelial cells

118   (IHCs) using a combination of tools including gene expression analysis, flow cytometry

119   and immunofluorescence staining (Fig. 1A). Phenotypic assessment was performed on

120   thawed biliary cells that were expanded on collagen type I coated plates for up to 4

121   passages. We first performed flow cytometry analysis to assess the homogeneity of

122   these cell populations, as well as the degree of mature protein marker expression. As

123   expected, the majority of IHCs expressed biliary markers SRY-related HMG transcription

124   factor 9 (SOX9), cytokeratin 7 (CK-7), cystic fibrosis transmembrane conductance

4

125 regulator (CFTR), and a subset were positive for epithelial cell adhesion molecule
126 expression (EpCAM). In contrast with stem cell-derived sources, IHCs expressed low
127 levels of the mature marker somatostatin receptor 2 (SSRT-2), a mediator of hormonal
128 signals during digestion, and did not exhibit alpha-fetoprotein (AFP), a common marker
129 expressed by progenitors (Fig. 1B).

130

131 We observed that cultured IHCs exhibited polygonal morphology, with visible cell-cell
132 adhesions (Fig. 1C). While IHCs initially grew as distinct patches with regular borders,
133 after multiple passages they began to exhibit elongated and spindle-like morphologies,
134 indicative of epithelial to mesenchymal transition, and acquired some fibroblastic features
135 such as fibronectin deposition while maintaining a degree of junctional marker expression
136 (Supplementary Fig. S1). Based on this observation, IHCs were not used for functional
137 studies beyond five passages. Immunofluorescence microscopy was used to visualize
138 the localization and expression of proteins common to epithelial and cholangiocyte
139 identity, namely membrane bound cell-cell adhesion marker β-Catenin, cytoplasmic
140 cytokeratin 19 (CK-19) and nuclear biliary markers hepatic nuclear factor - 1β (HNF-1β)
141 and SOX9 (Fig. 1C). Zinc metalloenzymes alkaline phosphatase (ALP) and γ-glutamyl
142 transpeptidase (GGT) are present in nearly all tissues but are enriched in biliary
143 epithelium *in vivo* and we observed that this population of IHCs demonstrate these
144 functional features (Fig. 1C, D; Supplementary Fig. S1). Through the collective analysis
145 of protein expression and enzymatic activity, we presume that the IHC population consists
146 mainly of large rather than small cholangiocytes, evidenced by CFTR expression and
147 GGT and ALP activity [32].

148

149
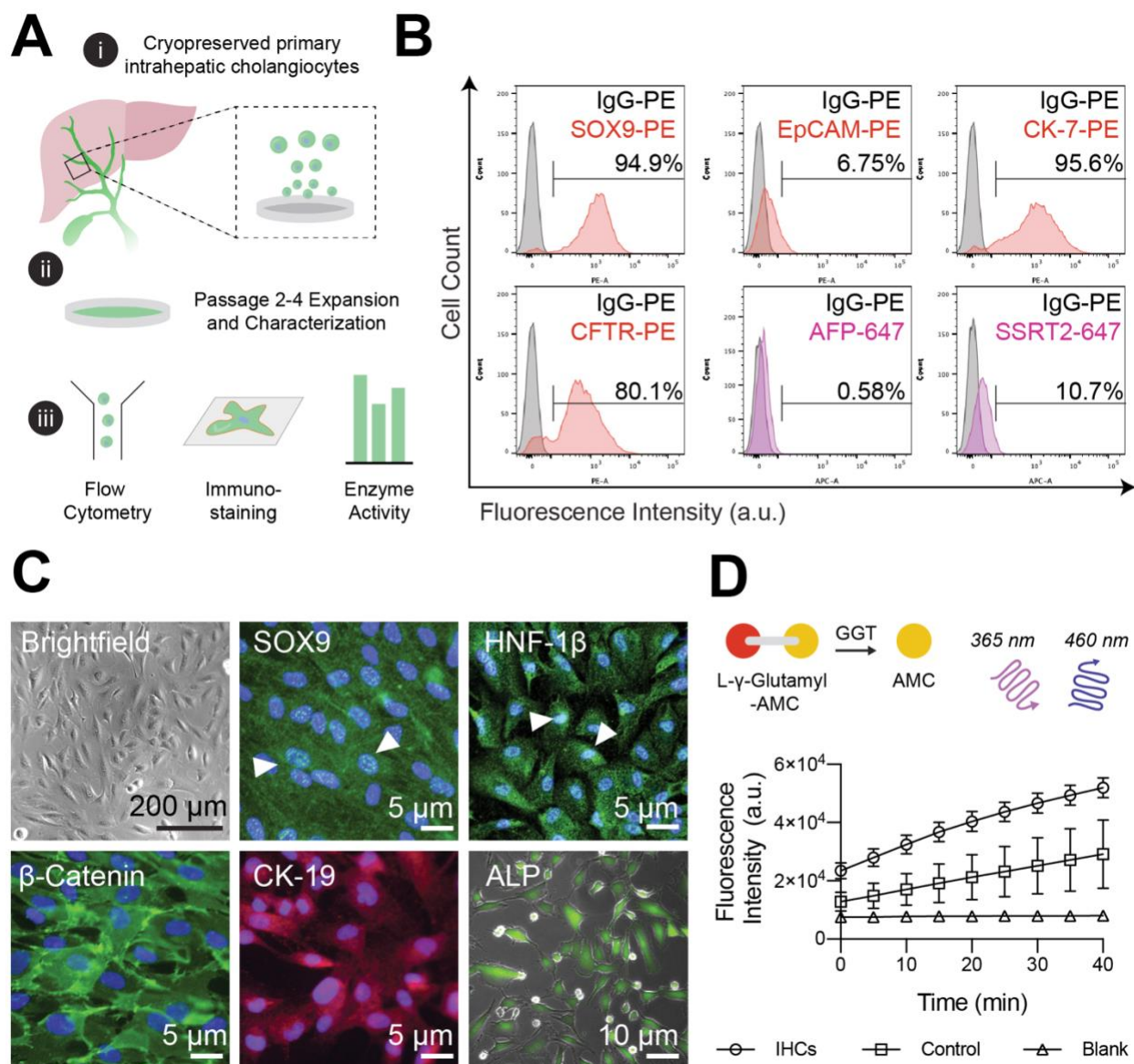
Figure 1. Characterization of primary intrahepatic cholangiocytes. (A) (i) Schematic describing the approach to characterize adult, cryopreserved primary human intrahepatic cholangiocyte (IHCs); (ii) IHCs were expanded on collagen-coated plates and used for up to four passages; (iii) Passage 2 IHCs were characterized with a combination of flow cytometry analysis, immunofluorescence staining, and enzymatic activity assays. **(B)** Representative flow cytometry histogram plots showing SOX9, EpCAM, CK-7, CFTR, AFP and SSRT2 expression compared to IgG isotype controls (in gray; [n = 3]). **(C)** Representative brightfield and epi-fluorescence images of IHCs cultured on collagen-coated substrates (n = 3 biological replicates). IHCs show nuclear localization of SOX9 and HNF-1β expression (green signal overlapping with nuclear DAPI stain in blue; white arrows), and positive cytoplasmic expression of β-catenin (green) and CK-19 (red). IHCs were incubated with a live alkaline phosphatase (ALP) stain for 30 minutes, washed with serum-free media and imaged with fluorescence microscopy (Nuclei were stained with DAPI). **(D)** γ-glutamyl transferase activity (GGT) measured using a colorimetric assay

165 where time course of fluorescence intensities is shown, denoting the liberation of 7-
166 Amino-4-Methyl Coumarin (AMC) from a γ-glutamyl quenched substrate. Graphs
167 represent mean and standard deviation from technical triplicates with blank and GGT
168 positive controls.
169

170 **Composite Extracellular Matrices Promote Cholangiocyte Branching in 3D Culture**

171

172 After validating that IHCs exhibit a collective set of phenotypic and functional traits, we

173 proceeded to leverage insight from *in vivo* developmental studies to assay whether these

174 cholangiocyte-like cells can self-assemble into biliary networks *in vitro*. We hypothesized

175 that IHCs would have the ability to form interconnected 3D branched network structures

176 within a native extracellular niche, given the appropriate introduction of matrix and

177 chemical cues. To this end, we first fluorescently labeled IHCs using a puromycin-

178 selective lentiviral red fluorescent protein (RFP) system, designed to visualize live F-actin

179 expression. Next, after selection via antibiotic resistance, we expanded and

180 encapsulated the resulting Life-Act RFP-IHCs at a density of $1x10^6$ cells/mL in either

181 Matrigel or Matrigel/ collagen type 1 blends. Four days post encapsulation, we fixed and

182 labeled the nuclei of resulting structures, imaged using confocal microscopy, and

183 performed image analysis on z-plane maximum intensity projections. To evaluate the

184 resulting morphological features, we used a computer algorithm to segment image

185 attributes and quantified network coverage, branch points, and structure lengths (Fig. 2A).

186

187 IHCs that were encapsulated in growth factor-reduced Matrigel were incubated with or

188 without EGF stimulation and exposed to conditions with L-685,458, a potent and selective

189 γ-secretase inhibitor that blocks Notch transcriptional activity [33]. IHCs cultured in pure

190 Matrigel scaffolds without EGF stimulation produced limited sprouting and formed large

191 aggregate structures, with multiple branched features extending from the clustered core.

192 With Notch inhibition, cell aggregation diminished, indicative of increased matrix

193 interaction compared to homotypic cell-cell interactions. However, multi-cellular

194 branched features were not identified (Supplementary Fig. S2). Sprouting behavior in

195 Matrigel improved in the presence of 20 ng/mL EGF, demonstrating the role of mitogen

196 stimulation on biliary branching in laminin rich matrices (Supplementary Fig. S2)**.**

7

197

198   We hypothesized that the addition of fibrillar architecture within Matrigel could promote

199   biliary sprouting behavior. Therefore, we created composite gels consisting of Matrigel

200   and 3.0 mg/mL rat tail collagen type I and assessed IHC sprouting behavior under EGF

201   stimulation and Notch inhibition. While there were no significant differences in the number

202   of branch points, branch length, or percent coverage of IHCs cultured in 3D composite

203   gels with 0 ng/mL EGF with or without Notch inhibition, we found that the addition of 20

204   ng/mL EGF had a significant impact on the potential to form interconnected branched

205   features. Notably, we observed an increase in the density and number of observed

206   branched points (Fig. 2B i, ii). We also evaluated the combinatorial role of co-

207   administering hepatocyte growth factor (HGF) with EGF on IHC branching potential, as

208   they both have been implicated in inducing ductal morphogenesis during development

209   (Supplemental Fig. S3A). We found that HGF alone can also support IHC sprouting, but

210   the combination with HGF and EGF leads to densely interconnected structures. Again,

211   when Notch inhibition is introduced, the additive effects of HGF and EGF are abrogated,

212   implicating a strong role for Notch signaling in branching morphogenesis (Supplemental

213   Fig. S3B, C).

214

215   We next appraised network functionality through analysis of ATP-dependent flux. The

216   multidrug resistance 1 (MDR1) P-glycoprotein protects cholangiocytes from toxic cationic

217   agents present in hepatocyte-secreted bile acid, including xenobiotic substances or

218   drugs. Rhodamine 123 is a fluorescent tracer dye and substrate of MDR1 and is actively

219   transported into the lumen of biliary epithelial cells. 3D incubation of Rhodamine 123 in

220   20 ng/mL EGF-stimulated networks led to secretory functionality, with a lumenal influx of

221   the fluorescent substrate (Fig. 2C). We were also able to identify lumen within the

222   branching cholangiocytes using high-resolution confocal microscopy (Fig. 2D). For a

223   controlled evaluation of the role of growth factor presentation during IHC branching, we

224   chose to specifically look at EGF stimulation in 3D culture conditions, but also compared

225   these effects to IHCs cultured as 2D monolayers (Supplementary Figure S4). To

226   elucidate the effects of EGF on known Notch signaling targets, IHC transcript levels were

227   measured in 3D composite gels cultured with 0, 20, or 50 ng/mL EGF. Our analysis

228   revealed that EGF stimulation affected *GGT*, *JAG1*, *NOTCH2*, and *HES1* mRNA

229   expression levels in a dose-dependent manner and elicited a significant increase in

230   *NOTCH2* gene expression with 20 ng/mL EGF stimulation (Fig. 2E).
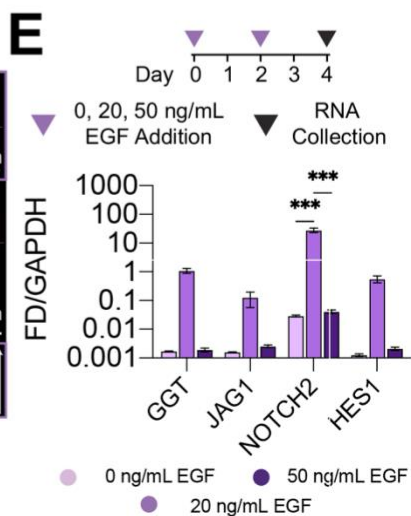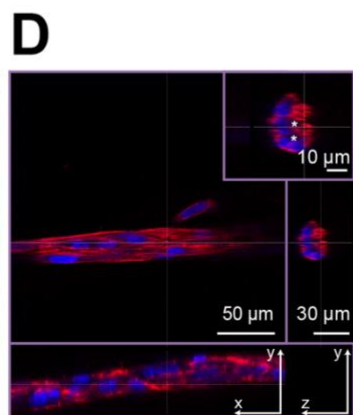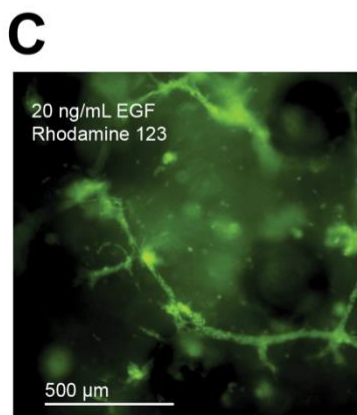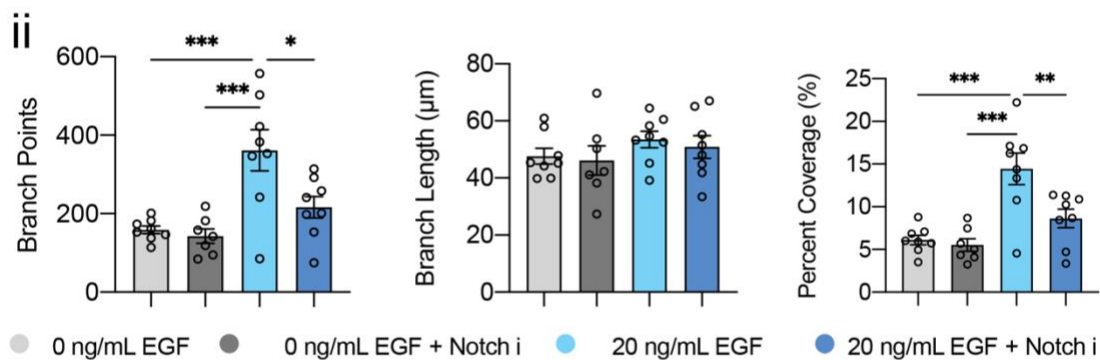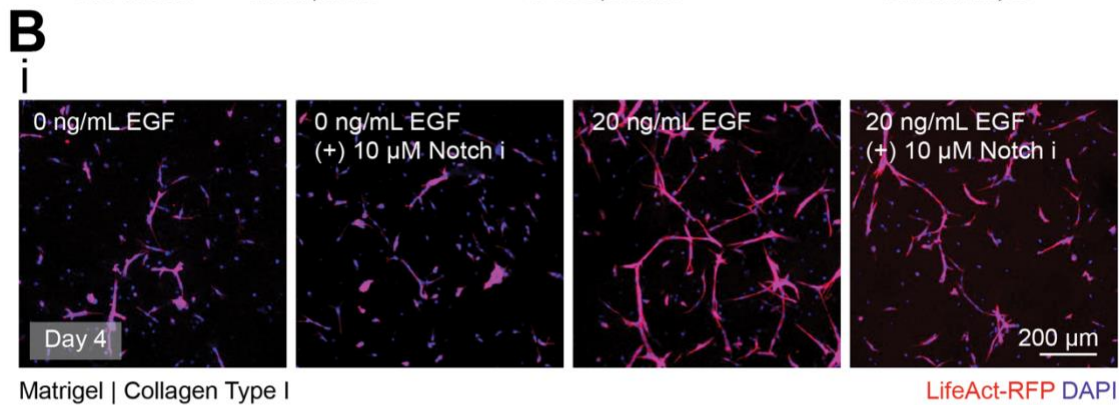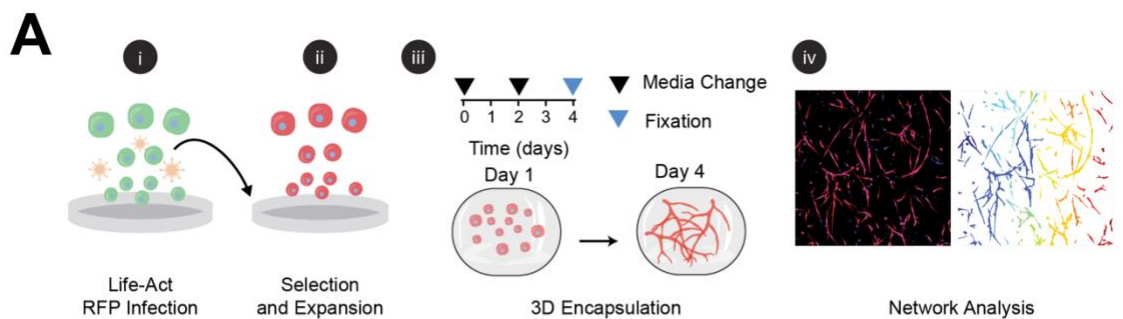
Figure 2. Composite Matrigel and Collagen Type I Gels Support Cholangiocyte Branching Morphogenesis. (A) Experimental schematic to probe the capacity for primary human intrahepatic cholangiocytes to undergo branching morphogenesis: (i) Fluorescence tagging of IHCs by rLVUbi-LifeAct-TagRFP cytoskeletal labeling; (ii) A homogenous population of IHCs stable for red fluorescence protein (RFP) expression of F-actin was generated after puromycin selection and expanded in cholangiocyte media; (iii) Resulting populations were encapsulated in Matrigel/collagen type 1 gels for four days, and (iv) features of branching morphologies were measured from maximum intensity z-projections of confocal images using a segmentation algorithm. **(B)** (i) Representative images of LifeAct RFP-IHCs encapsulated in Matrigel/Collagen I blends, cultured with and without EGF or Notch inhibition (10 µM L,685,458). (ii) Individual data points of quantified branch length, points, and network percent coverage. P-values were obtained using One-Way ANOVA Tukey's hypothesis testing. Representative images generated from at least 7 independent fields of view from 3 biological replicate experiments. At least 20 segmented features were analyzed per field of view. **(C)** Functional uptake of Rhodamine 123 after 4 days of IHC culture in Matrigel/collagen type 1 blends containing 20 ng/mL of EGF. **(D)** F-actin stain of cholangiocytes grown in Matrigel/collagen type 1 composites after 4 days with 20 ng/mL EGF stimulation. White asterisks in the cross-section indicate lumen within the branched structures **(E)** mRNA expression levels of *GGT* and Notch signaling genes measured via RT-qPCR for IHCs four days post 3D culture. Bar graphs show internal triplicate measurements from the pooled collection of 5 biological replicate gels. P-values were obtained using Two-Way ANOVA Tukey's hypothesis testing. $P < 0.033$ (*), $P < 0.002$ (**), $P < 0.001$ (***). All data represented as mean $\pm$ SEM.

EGF Stimulation Enhances Notch Signaling During Cholangiocyte Branching

We engineered Notch2-deficient cells using CRISPR/Cas9 (Clustered Regularly Interspaced Short-Palindromic Repeats/ CRISPR associated protein 9) mediated deletion to further validate EGF's role in Notch signal transduction and IHC branching potential. In brief, two guide RNAs (gRNAs; Scramble control, and Notch2) were cloned into puromycin-sensitive lentiviral CRISPR/Cas9 vectors and packaged with HEK293 cells. The resulting complexed particles were used to infect freshly thawed IHCs (Fig. 3A). Relative protein levels of the Notch2 intracellular domain (Notch2-ICD) were confirmed via western blot analysis of cell lysates, showing decreased expression in Notch2 knockdown (KD) compared to scrambled control cells (Fig. 3B). These changes were consistent at the mRNA level (Fig. 3C), reflecting a broad uptake of the CRISPR-mediated deletion, despite some residual, Notch2-intact cells remaining in the population. Finally, cells from the control and Notch2 depleted populations were encapsulated in

271 Matrigel/collagen type 1 composite gels with 20 ng/mL EGF stimulation. After 4 days, the

272 Notch2-depleted population exhibited dramatically blunted sprouting potential, relative to

273 the scrambled control cells (Fig. 3D). These results confirm the role of EGF in the Notch

274 signaling axis in IHCs, which presumably mediates branching morphogenesis in

275 composite natural scaffolds.

276
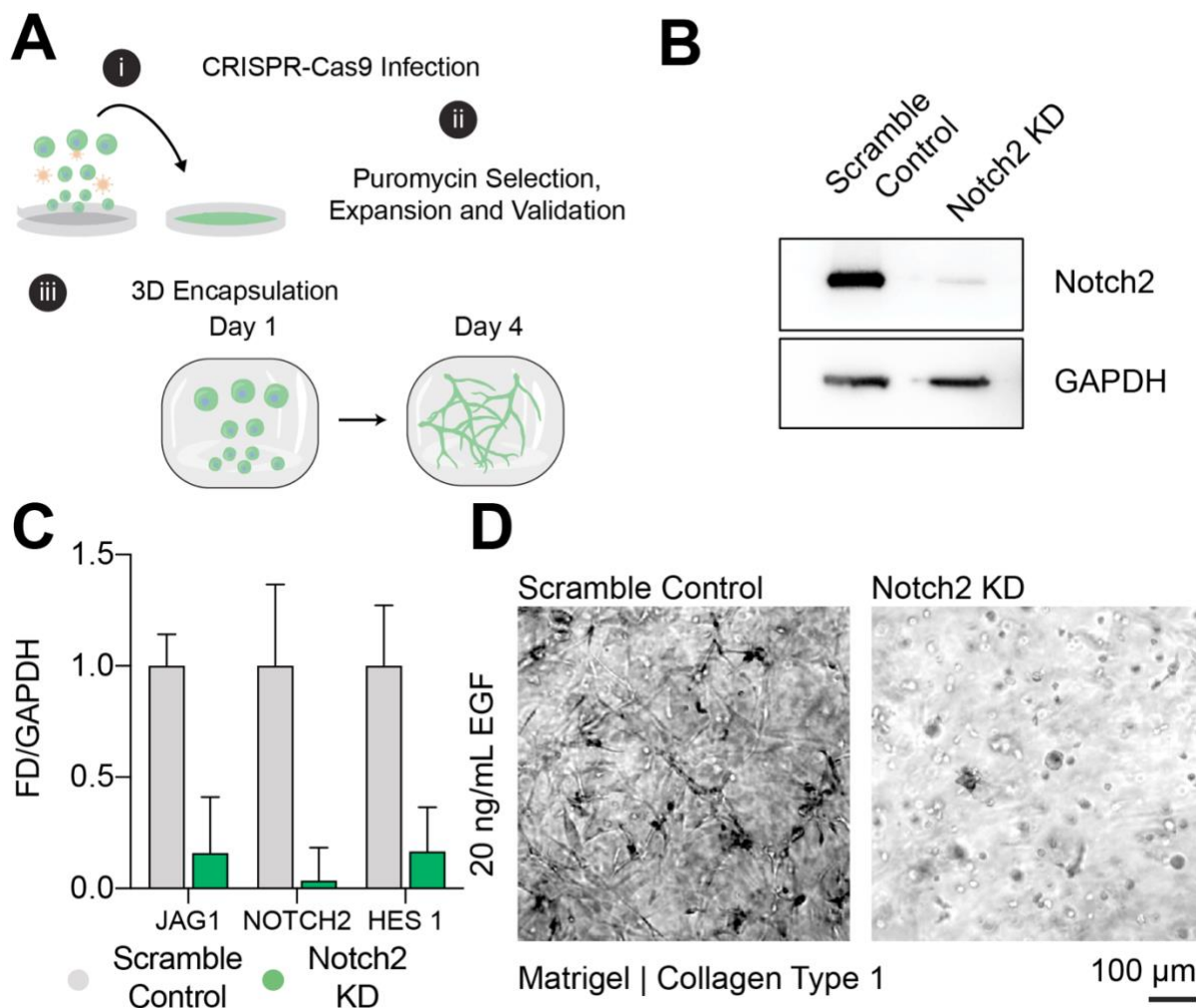
277

278 **Figure 3. CRISPR-Cas9 Mediated Notch2 Knockdown Ablates Cholangiocyte**
279 **Branching Morphogenesis in Hydrogel Blends. (A)** Schematic of the workflow to test
280 the impact of Notch2 knockdown in cholangiocyte branching morphogenesis. **(B)** Notch
281 2 intracellular domain (Notch 2 – ICD) downregulated protein expression in Notch 2
282 knockdown (KD) IHCs compared to scramble control cells. **(C)** Comparison of mRNA
283 expression between scramble control and Notch2 KD cells. Notch2 KD cells show
284 downregulation of *JAG1*, *NOTCH2*, and *HES1* gene expression compared to scramble
285 controls (n = 2). **(D)** Brightfield images of scramble control and Notch2 KD cells grown in

12

286 Matrigel/ collagen I hydrogel blends after four days. Notch2 KD cholangiocytes show
287 blunted branching compared to control cells (n=3, triplicate gels).
288

Intrahepatic Biliary Tree on a Microfluidic Chip

290

291 To demonstrate IHC sprouting potential in a system amenable to flow, which allows the

292 study of biliary phenotypes in a dynamic, physiologically relevant microenvironment, we

293 leveraged a previously developed microfluidic platform [27,34]. In brief, the

294 polydimethylsiloxane (PDMS)-based device contains guide features when bonded on a

295 coverslip, allowing for the insertion of parallel needles (300 μm in diameter, spaced 1 mm

296 apart). Subsequent to needle insertion, prepolymer solutions with or without cells can be

297 introduced within the device. After the polymer has crosslinked, needle removal leaves

298 open structures that can be seeded with cells, allowing for bulk cellular self-assembly and

299 prefabricated vessel-shaped structures (Fig. 4A). We first leveraged insight from our bulk

300 3D culture experiments, and mixed IHCs in pre-polymerized composite gels into the

301 device. Following polymerization and needle removal, we seeded additional IHCs into

302 the lumen of the channels via a pressure differential and cultured the devices under

303 gravity-driven perfusion using a rocker platform. After monitoring RFP expression over

304 the course of 6 days, we found that the vessel structures collapsed into cords, blunting

305 channel access for perfusion, but permitted the assembly of branching architectures in

306 the bulk of the device (Fig. 4B). When comparing this observed phenotype to microfluidic

307 culture of normal rat cholangiocytes (NRCs), we found that Matrigel/collagen blends

308 supported both bulk cystic morphogenesis and sustained polarized cell-laden channels

309 as previously described (Supplementary Figure S5)[19]. NRC culture inside the fluidic

310 channels phenocopies the epithelial polarization we expect in normal biliary epithelium,

311 including strong junctional marker expression. However, to maintain patent vessel

312 architecture with the IHCs, we explored the use of alternative biomaterial scaffolds. We

313 found that fibrin, a sticky clotting agent comprised of fibrinogen and thrombin, enhanced

314 biomaterial adhesion to the glass and PDMS features of the device, sustaining both

315 patent cholangiocyte-lined ducts as well as dense, interconnected branched features (Fig.

316 4C). Collectively, these results demonstrate the capacity to form a biliary tree on a

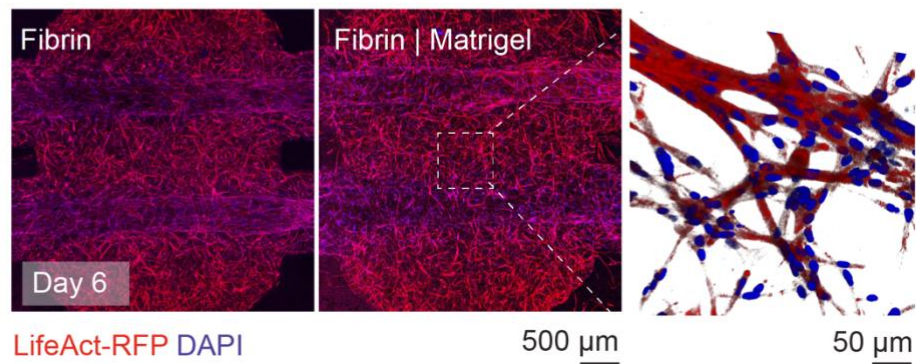317 microfluidic chip that is amenable to the introduction of flow.

13

318
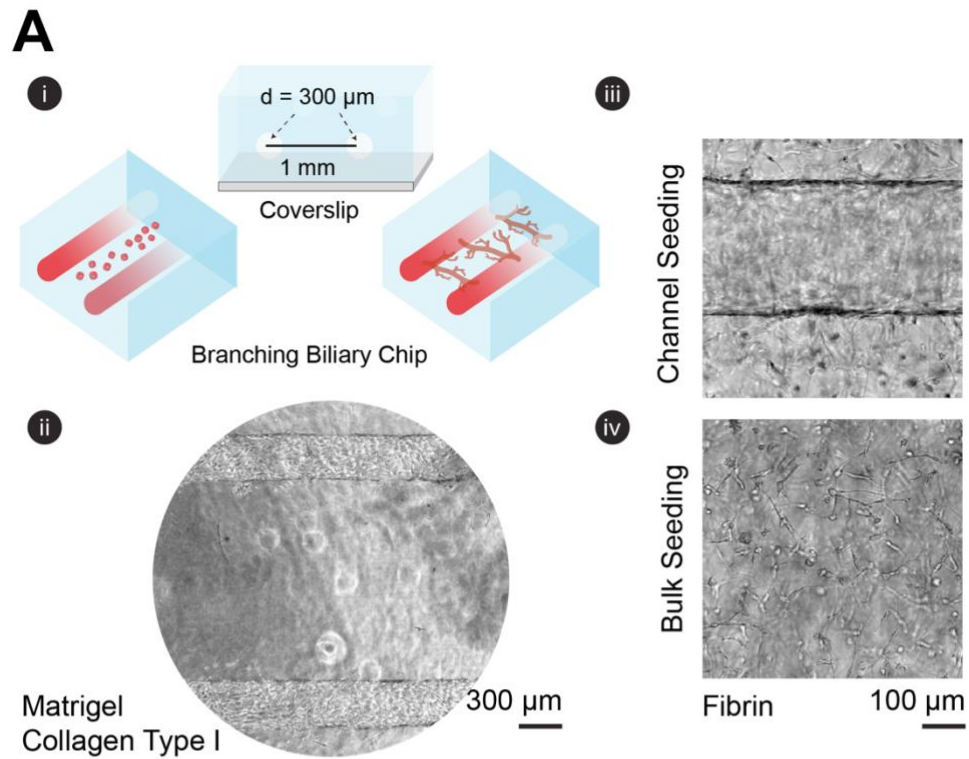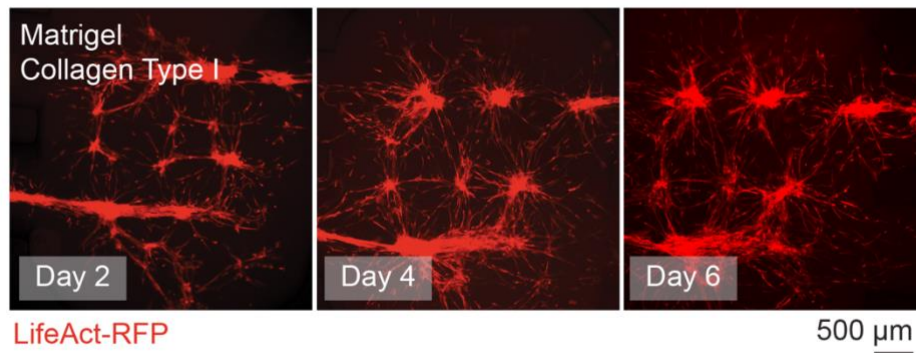
319

320 **Figure 4. Hierarchical Intrahepatic Biliary Duct on a Chip. (A)** (i) Device schematic
321 and representative brightfield images, showing top and cross-sectional views of a dual
322 channel microfluidic platform; (ii) encased within the biomaterial scaffolds are two parallel
323 300 µm open lumenal structures spaced 1 mm apart; (iii) the arrangement provides
324 capacity to seed IHCs and flow media in the patent channels; (iv) and encapsulate IHCs
325 in the bulk compartment of the device. **(B)** Representative time course images of LifeAct
326 RFP-IHCs grown in microfluidic device with 20 ng/mL EGF, showing collapse of open
327 structures after six days, but anastomosis between bulk networks with channel structures.
328 **(C)** Representative maximum intensity projection images of LifeAct RFP-IHCs cultured
329 for 6 days with 20 ng/mL EGF in fibrin scaffolds, showing maintenance of open cell-laden
330 channels compared to Matrigel/collagen type 1 scaffolds (Nuclei stained with DAPI).
331

332 **DISCUSSION**

333

334 Here we describe a pipeline for characterizing primary human biliary isolates and

335 appraised their functional and morphogenic potential under controlled *in vitro*

336 microenvironments. We specifically show that extracellular matrix composition, growth

337 factor presentation, and Notch activity elicit the self-assembly of branched epithelial

338 structures that mimic native biliary tissue. The resulting structures maintain

339 cholangiocyte-specific function and are able to transport multiple drug resistance protein

340 substrates. Furthermore, we successfully combined top-down and bottom-up

341 approaches to engineer large (300 µm) cholangiocyte-lined channels as well as smaller

342 self-assembled branched cholangiocyte networks in a microfluidic platform. We envision

343 that this engineered 'chip' format can be leveraged for future evaluation of shear stress,

344 permeability, and spatially organized co-cultures. Collectively, these results reinforce

345 approaches that can be used to study cell-cell and cell-matrix during tissue

346 morphogenesis and provides a strategic framework for future integration of biliary

347 epithelium in existing engineered liver platforms [35,36].

348

349 Notch signaling is an evolutionarily conserved intracellular pathway that regulates many

350 aspects of embryonic development including cell-fate specification and morphogenesis.

351 Consequently, dysregulation of Notch signaling can lead to an array of developmental

352 disorders that affect many tissues including the liver. Mammalian cells contain four

353 different single pass transmembrane Notch receptors (NOTCH 1-4). Upon ligand

354 engagement by neighboring Jagged or Delta-like protein expressing cells, the

15

355   extracellular domain of the Notch receptor undergoes proteolytic cleavage by an ADAM

356   metalloprotease. Following this reaction, cleavage of the Notch intracellular domain

357   (NICD) by γ-secretase, liberates the protein to translocate to the nucleus where it interacts

358   with the recombination signal binding protein for immunoglobulin kappa J (RBPJ)

359   transcription factor. This association promotes downstream expression of hairy and

360   enhancer of split-1 (HES1) which acts to confer instructions to neighboring cells during

361   embryonic patterning. Notch signaling is essential to bile duct specification and

362   subsequent tubule formation [37], and patients with Alagille syndrome, contain inherited

363   mutations in either the Notch2 receptor or Jag1 ligand resulting in cholestasis from ductal

364   paucity[38]. Kitade et al. show mouse derived bipotential hepatic progenitor cells (HPCs)

365   undergo cholangiocyte specification and branching morphogenesis in Matrigel/collagen I

366   gels. This branching is mediated by EGFR and MET stimulation using EGF and HGF

367   media supplementation, respectively. *EGFR* null HPCs are unable to undergo branching

368   morphogenesis or acquire biliary marker expression upon growth factor addition [39].

369   Furthermore, *EGFR* competent HPCs with Notch deletion fail to differentiate or branch

370   with MET/EGFR activation. In line with these results, our human *in vitro* system

371   corroborates the crosstalk between Notch/EGF (EGFR) signal transduction in biliary

372   morphogenesis [37,40].

373

374   We show that inhibition of γ-secretase by L-685,458 or knockdown of Notch2 via

375   CRISPR/Cas9, leads to reduced branching morphogenesis *in vitro* and abrogates

376   transcriptional activation of *HES1*. Furthermore, we find that EGF stimulation during

377   branching morphogenesis is correlated with increased Notch signal transduction,

378   evidenced by the upregulation of *HES1*. We find that this transcriptional regulation of

379   Notch activity is specific to 3D culture conditions. Whether this phenotype is regulated by

380   ECM stiffness has yet to be elucidated, but mechanical forces have been demonstrated

381   to regulate YAP/TAZ control of Notch activation in epidermal stem cells [41]. Additionally,

382   bi-potent mouse hepatoblasts have been shown to preferentially differentiate into

383   cholangiocytes at the periphery of circular micropatterned domains. Compared to central

384   areas, these regions elicit increased actomyosin stress and elevate *NOTCH2* and *JAG1*

385   transcriptional activity [42]. Applying these principles to our system, we stipulate that

16

386   rheological characterization of our optimized matrices will provide additional insight into

387   the role of scaffold mechanics on Notch-mediated morphogenesis.

388

389   Aside from standardizing media components, differences in the described morphogenic

390   potential of varying cholangiocytes should be reconciled by transcriptional profiling, which

391   allows for stratification of specie specific phenotypes. In addition, single cell analysis can

392   illuminate functional differences between stem cell-derived, adult progenitor and small/

393   large cholangiocyte subtypes [43]. Finally, while immortalized cell lines have proven useful

394   for *in vitro* mechanistic studies, questions regarding their phenotypic stability,

395   tumorgenicity and transcriptional landscape remain, limiting their clinical utility for

396   regenerative medicine applications.   Our system provides an important framework for

397   directing primary human biliary assembly that can be integrated with existing approaches

398   in liver tissue engineering. There are notable limitations in this system, including the need

399   for further functional validation of the cholangiocyte-like cells used in this study. For

400   example, optimization of culture conditions should be conducted to limit mesenchymal

401   features after serial passage and investigation of other markers such as the sodium-

402   dependent bile acid transporter (ASBT) and osteopontin (OPN) should be pursued. With

403   this described microfluidic system, one can measure cholangiocyte permeability,

404   response to small molecules (ATP and acetylcholine stimulation on calcium influx

405   dynamics), shear stress, and varying bile compositions.   While we demonstrate the role

406   of EGF stimulation on Notch signaling, other signal transduction pathways such as

407   PI3K/Akt and MEK/ERK intracellular pathways can be affected by EGF as well.

408   Furthermore, tethering EGF ligands to the scaffolds, rather than bulk administration, could

409   lead to enhanced signal transduction and morphogenetic processes [44] . In summary, we

410   provide insight into growth factor-mediated branching in liver epithelium, consistent with

411   findings in lung or kidney morphogenesis, but unveil tissue-specific ligand-receptor

412   feedback between EGF and Notch signaling. Leveraging this insight, we directed the

413   assembly of biliary duct structures using a microfluidic platform, adding a new model

414   system of the portal triad.

415

416

17

417 **ACKNOWLEDGEMENTS**

418

431

18

432

MATERIALS AND METHODS

434

Primary Human Biliary Epithelial Cell Culture. Human intrahepatic biliary epithelial cells (IHCs) passage 1-5 (ScienCell, Carlsbad, CA) were cultured in complete epithelial growth media (ScienCell) on 50 µg/mL type I collagen coated surfaces (Corning). IHCs were isolated from human liver tissue using mechanical dissociation and enriched for CK-19. Media was exchanged every two to three days, passaged at 80% confluency with 0.05% trypsin/EDTA (ThermoFisher Scientific, Waltham, MA), and maintained in a humidified 5% CO_2 incubator at 37ºC.

442

Flow Cytometry. Marker expression was verified through cytometry, where PE or APC-conjugated antibodies were stained on fixed and permeabilized cells. To harvest cells for flow analysis, serum was removed prior to adding TrypLE (Invitrogen, Waltham, MA) dissociation buffer, by washing with 1x PBS. After collection, cells were fixed with 3.7% paraformaldehyde (PFA) for 5minutes, spun for 2 minutes at 200xG, and resuspended in 0.1% Triton X for 10 minutes. Cells were then incubated in 100 µl of 0.1% bovine serum albumin (BSA; Sigma-Aldrich, St. Louis, MO) in PBS with conjugated antibodies for 1 hour at room temperature. Cells were washed three times to reduce non-specific staining and analyzed on a BD LSRFortessa (BD Biosciences, Franklin Lakes, NJ). To determine levels of expression, all analyses were conducted using IgG-PE or IgG-APC (BD) isotype controls.

454

Immunofluorescence Staining and Imaging. Cells cultured on glass collagen I coverslips, were washed with 1X PBS and fixed in 3.7% paraformaldehyde for 10 minutes. After washing the samples with 1X PBS, samples were incubated in 0.1% Triton X-100 (Sigma-Aldrich) for 10 minutes. Next, cells were washed with 1X PBS and incubated for 1 hour at room temperature in 1% BSA to block for non-specific binding. Samples were then incubated with primary antibodies diluted in 1X overnight at 4ºC, washed with incubated with secondary antibodies for 1 hour at room temperature. Finally, samples were incubated with Hoechst solution (ThermoFisher) for 3 minutes and washed

463   with PBS prior to imaging. Cell morphology was identified using a Nikon TE200 Inverted

464   microscope.

465

466   **Biochemical Assays.** γ-Glutamyl Transferase activity was acquired using the

467   Colorimetric Assay Kit (Sigma-Aldrich). In brief, 1 million, IHCs and fibroblast controls

468   were collected in microcentrifuge tubes. Cells were pelted by spinning down at 200 x G

469   for 3 minutes. After aspirating out the supernatant, cells were resuspended in 200 µl of

470   cold GGT Assay Buffer and spun at 13,000 x G for 10 minutes.   Activity was acquired

471   through kinetic absorbance measurements (418 nm) at 37⁰C using a TECAN Infinite

472   microplate reader.   To determine alkaline phosphatase (ALP) activity, growth media of

473   live cell cultures was removed, prior to washing vessels with pre-warmed DMEM/F-12.

474   Adherent cells were then incubated for 20-30 minutes with a 1X ALP Live Stain solution

475   (ThermoFisher). After incubation, the ALP solution was removed, and cultures were

476   washed two times with fresh DMEM/F-12 for 5 minutes per wash prior to imaging using

477   FITC illumination.

478

479   **Biliary Network Formation.** Collagen gels were formed as previously described. In brief,

480   1.0x10^6 cells/mL were encapsulated in gels composed of Matrigel mixed at equal parts

481   with 3.0 mg/mL rat tail collagen type I, that was titrated to pH 7.0-7.5 with 1M NaOH. 100

482   µl of the collagen mixture was added to wells of a 96 well plate and allowed to polymerize

483   at 37⁰C for 30 minutes. After the gel solidified, an additional 100 µl of supplemented

484   epithelial media was added.

485

486   **Biliary Network Quantification.** A custom image processing program was written in

487   MATLAB (Natick, MA) to quantify morphological features of branching phenotypes.

488   Maximum intensity projections of confocal z-stacks were processed using ImageJ (NIH).

489   Next, images were exported as JPEG files and imported into MATLAB. Red fluorescent

490   protein (RFP) signal was used to identify network features. Masked image segments

491   were enumerated and evaluated for percent coverage, branch length, and branch points.

492

493   **Quantitative Reverse-Transcription PCR.** Total RNA was extracted using TRIzol

494   Reagent (Invitrogen) from IHCs cultured under varying conditions. Quality and quantity

495   of extracted RNA was verified by NanoDrop spectrophotometry prior to implementation

496   of the 1 step RNA to Ct kit (ThermoFisher). Each measurement was conducted in

497   triplicate with non-template controls using a BioRad CFX96 instrument. GAPDH served

498   as endogenous controls for global normalization to acquire mRNA expression. Reference

499   groups for differential analysis are outlined in the text and fold differences were calculated

500   by the comparative Ct method.

501

502   **Lentiviral-Mediated CRISPR Genome Editing.** CRISPR knockdown cells were

503   generated using the lentiCRISPRv2 system (gift of F. Zheng, Addgene plasmid #52961).

504   Scramble guideRNA (gRNA) (GCACTACCAGAGCTAACTCA) and NOTCH2 gRNA

505   (GGCGCTCTGGCTGTGCTGCG) were designed using the Optimized CRISPR Design

506   tool (F. Zheng, MIT) and cloned into the BsmBI site of plentiCRISPRv2. gRNA-containing

507   pLentiCRISPR plasmids were co-transfected with pVSVG, pRSV-REV, and pMDL

508   packaging plasmids into HEK-293T cells using calcium phosphate transfection. After 48

509   hours, viral supernatants were collected, concentrated using PEG-IT viral precipitator

510   (SBI), and resuspended in PBS. Cells were transduced in growth medium overnight and

511   selected with 2 µg/ml puromycin 48 h after infection. CRISPR modifications were verified

512   by western blot.

513

514   **Western and Immunoblotting.** Cell lysates were prepared with equal amounts of total

515   protein (as measured using the Pierce Coomassie protein assay reagent) and separated

516   on a NuPage Bis-Tris gels, transferred to PVDF (ThermoFisher), blocked in 5% milk and

517   subjected to Western blot analysis using antibodies for Notch2 (Cell Signaling, D76A6)

518   and GAPDH (Cell Signaling, D16H11). The blots were developed using ECL Western blot

519   detection reagents (Pierce), and the signal was detected on iBrightTM CL1500 Imaging

520   System (ThermoFisher).

521

522   **Quantification and Statistical Analysis.** All statistical analysis was performed in

523   GraphPad (Prism 9.0). Statistical significance was determined via methods outlined in

524   the figure legends.

525

526

REFERENCES:

1. Song, H. G., Lammers, A., Sundaram, S., Rubio, L., Chen, A. X., Li, L., Eyckmans, J., Bhatia, S. N., & Chen, C. S. (2020). Transient Support from Fibroblasts is Sufficient to Drive Functional Vascularization in Engineered Tissues. *Advanced Functional Materials*, *30*(48), 2003777. https://doi.org/10.1002/adfm.202003777

2. Stevens, K. R., Ungrin, M. D., Schwartz, R. E., Ng, S., Carvalho, B., Christine, K. S., Chaturvedi, R. R., Li, C. Y., Zandstra, P. W., Chen, C. S., & Bhatia, S. N. (2013). InVERT molding for scalable control of tissue microarchitecture. *Nature Communications*, *4*(1), 1847. https://doi.org/10.1038/ncomms2853

3. Stevens, K. R., Scull, M. A., Ramanan, V., Fortin, C. L., Chaturvedi, R. R., Knouse, K. A., Xiao, J. W., Fung, C., Mirabella, T., Chen, A. X., McCue, M. G., Yang, M. T., Fleming, H. E., Chung, K., Jong, Y. P. de, Chen, C. S., Rice, C. M., & Bhatia, S. N. (2017). In situ expansion of engineered human liver tissue in a mouse model of chronic liver disease. *Science Translational Medicine*, *9*(399), eaah5505. https://doi.org/10.1126/scitranslmed.aah5505

4. Baranski, J. D., Chaturvedi, R. R., Stevens, K. R., Eyckmans, J., Carvalho, B., Solorzano, R. D., Yang, M. T., Miller, J. S., Bhatia, S. N., & Chen, C. S. (2013). Geometric control of vascular networks to enhance engineered tissue integration and function. *Proceedings of the National Academy of Sciences*, *110*(19), 7586–7591. https://doi.org/10.1073/pnas.1217796110

5. Vroman, B., & LaRusso, N. F. (1996). Development and characterization of polarized primary cultures of rat intrahepatic bile duct epithelial cells. *Laboratory Investigation; a Journal of Technical Methods and Pathology*, *74*(1), 303–313.

6. Tabibian, J. H., Trussoni, C. E., O'Hara, S. P., Splinter, P. L., Heimbach, J. K., & LaRusso, N. F. (2014). Characterization of cultured cholangiocytes isolated from livers of patients with primary sclerosing cholangitis. *Laboratory Investigation*, *94*(10), 1126–1133. https://doi.org/10.1038/labinvest.2014.94

7. Loarca, L., Assuncao, T. M. D., Jalan-Sakrikar, N., Bronk, S., Krishnan, A., Huang, B., Morton, L., Trussoni, C., Bonilla, L. M., Krueger, E., O'Hara, S., Splinter, P., Shi, G., Pisarello, M. J. L., Gores, G. J., Huebert, R. C., & LaRusso, N. F. (2017). Development and characterization of cholangioids from normal and diseased human cholangiocytes as an in vitro model to study primary sclerosing cholangitis. *Laboratory Investigation*, *97*(11), 1385–1396. https://doi.org/10.1038/labinvest.2017.63

8. Huch, M., Dorrell, C., Boj, S. F., Es, J. H. van, Li, V. S. W., Wetering, M. van de, Sato, T., Hamer, K., Sasaki, N., Finegold, M. J., Haft, A., Vries, R. G., Grompe, M., & Clevers, H.

565   (2013). In vitro expansion of single Lgr5+ liver stem cells induced by Wnt-driven
566   regeneration. *Nature*, *494*(7436), 247–250. https://doi.org/10.1038/nature11826

567 9. Huch, M., Gehart, H., van Boxtel, R., Hamer, K., Blokzijl, F., Verstegen, M. M. A., Ellis, E.,
568   van Wenum, M., Fuchs, S. A., de Ligt, J., van de Wetering, M., Sasaki, N., Boers, S. J.,
569   Kemperman, H., de Jonge, J., Ijzermans, J. N. M., Nieuwenhuis, E. E. S., Hoekstra, R.,
570   Strom, S., … Clevers, H. (2015). Long-Term Culture of Genome-Stable Bipotent Stem Cells
571   from Adult Human Liver. *Cell*, *160*(1–2), 299–312. https://doi.org/10.1016/j.cell.2014.11.050

572 10. Sampaziotis, F., Brito, M. C. de, Geti, I., Bertero, A., Hannan, N. R., & Vallier, L. (2017).
573   Directed differentiation of human induced pluripotent stem cells into functional
574   cholangiocyte-like cells. *Nature Protocols*, *12*(4), 814–827.
575   https://doi.org/10.1038/nprot.2017.011

576 11. Tysoe, O. C., Justin, A. W., Brevini, T., Chen, S. E., Mahbubani, K. T., Frank, A. K., Zedira,
577   H., Melum, E., Saeb-Parsy, K., Markaki, A. E., Vallier, L., & Sampaziotis, F. (2019).
578   Isolation and propagation of primary human cholangiocyte organoids for the generation of
579   bioengineered biliary tissue. *Nature Protocols*, *14*(6), 1884–1925.
580   https://doi.org/10.1038/s41596-019-0168-0

581 12. Sampaziotis, F., Justin, A. W., Tysoe, O. C., Sawiak, S., Godfrey, E. M., Upponi, S. S.,
582   Gieseck, R. L., Brito, M. C. de, Berntsen, N. L., Gómez-Vázquez, M. J., Ortmann, D.,
583   Yiangou, L., Ross, A., Bargehr, J., Bertero, A., Zonneveld, M. C. F., Pedersen, M. T.,
584   Pawlowski, M., Valestrand, L., … Vallier, L. (2017). Reconstruction of the mouse
585   extrahepatic biliary tree using primary human extrahepatic cholangiocyte organoids. *Nature*
586   *Medicine*, *23*(8), 954–963. https://doi.org/10.1038/nm.4360

587 13. Ishii, M., Vroman, B., & LaRusso, N. F. (1989). Isolation and morphologic characterization
588   of bile duct epithelial cells from normal rat liver. *Gastroenterology*, *97*(5), 1236–1247.
589   https://doi.org/10.1016/0016-5085(89)91695-8

590 14. Tian, L., Deshmukh, A., Ye, Z., & Jang, Y.-Y. (2016). Efficient and Controlled Generation
591   of 2D and 3D Bile Duct Tissue from Human Pluripotent Stem Cell-Derived Spheroids. *Stem*
592   *Cell Reviews and Reports*, *12*(4), 500–508. https://doi.org/10.1007/s12015-016-9657-5

593 15. McAteer, J. A., Evan, A. P., & Gardner, K. D. (1987). Morphogenetic clonal growth of
594   kidney epithelial cell line MDCK. *The Anatomical Record*, *217*(3), 229–239.
595   https://doi.org/10.1002/ar.1092170303

596 16. Tanimizu, N., Miyajima, A., & Mostov, K. E. (2007). Liver Progenitor Cells Develop
597   Cholangiocyte-Type Epithelial Polarity in Three-dimensional Culture. *Molecular Biology of*
598   *the Cell*, *18*(4), 1472–1479. https://doi.org/10.1091/mbc.e06-09-0848

599 17. Lewis, P. L., Su, J., Yan, M., Meng, F., Glaser, S. S., Alpini, G. D., Green, R. M., Sosa-
600   Pineda, B., & Shah, R. N. (2018). Complex bile duct network formation within liver

24

601   decellularized extracellular matrix hydrogels. *Scientific Reports*, *8*(1), 12220.
602   https://doi.org/10.1038/s41598-018-30433-6

603   18. Funfak, A., Bouzhir, L., Gontran, E., Minier, N., Dupuis-Williams, P., & Gobaa, S. (2019).
604   Biophysical Control of Bile Duct Epithelial Morphogenesis in Natural and Synthetic
605   Scaffolds. *Frontiers in Bioengineering and Biotechnology*, *7*, 417.
606   https://doi.org/10.3389/fbioe.2019.00417

607   19. Du, Y., Khandekar, G., Llewellyn, J., Polacheck, W., Chen, C. S., & Wells, R. G. (2020). A
608   Bile Duct-on-a-Chip With Organ-Level Functions. *Hepatology*, *71*(4), 1350–1363.
609   https://doi.org/10.1002/hep.30918

610   20. Chen, C., Jochems, P. G. M., Salz, L., Schneeberger, K., Penning, L. C., Graaf, S. F. J. van
611   de, Beuers, U., Clevers, H., Geijsen, N., Masereeuw, R., & Spee, B. (2018). Bioengineered
612   bile ducts recapitulate key cholangiocyte functions. *Biofabrication*, *10*(3), 034103.
613   https://doi.org/10.1088/1758-5090/aac8fd

614   21. McGill, M. R., Williams, C. D., Xie, Y., Ramachandran, A., & Jaeschke, H. (2012).
615   Acetaminophen-induced liver injury in rats and mice: Comparison of protein adducts,
616   mitochondrial dysfunction, and oxidative stress in the mechanism of toxicity. *Toxicology and*
617   *Applied Pharmacology*, *264*(3), 387–394. https://doi.org/10.1016/j.taap.2012.08.015

618   22. Blais, E. M., Rawls, K. D., Dougherty, B. V., Li, Z. I., Kolling, G. L., Ye, P., Wallqvist, A.,
619   & Papin, J. A. (2017). Reconciled rat and human metabolic networks for comparative
620   toxicogenomics and biomarker predictions. *Nature Communications*, *8*(1), 14250.
621   https://doi.org/10.1038/ncomms14250

622   23. Martignoni, M., Groothuis, G. M. M., & Kanter, R. de. (2006). Species differences between
623   mouse, rat, dog, monkey and human CYP-mediated drug metabolism, inhibition and
624   induction. *Expert Opinion on Drug Metabolism & Toxicology*, *2*(6), 875–894.
625   https://doi.org/10.1517/17425255.2.6.875

626   24. Liu, Y., Meyer, C., Xu, C., Weng, H., Hellerbrand, C., Dijke, P. ten, & Dooley, S. (2013).
627   Animal models of chronic liver diseases. *American Journal of Physiology-Gastrointestinal*
628   *and Liver Physiology*, *304*(5), G449–G468. https://doi.org/10.1152/ajpgi.00199.2012

629   25. Odom, D. T., Dowell, R. D., Jacobsen, E. S., Gordon, W., Danford, T. W., MacIsaac, K. D.,
630   Rolfe, P. A., Conboy, C. M., Gifford, D. K., & Fraenkel, E. (2007). Tissue-specific
631   transcriptional regulation has diverged significantly between human and mouse. *Nature*
632   *Genetics*, *39*(6), 730–732. https://doi.org/10.1038/ng2047

633   26. Khetani, S. R., Berger, D. R., Ballinger, K. R., Davidson, M. D., Lin, C., & Ware, B. R.
634   (2014). Microengineered Liver Tissues for Drug Testing. *Journal of Laboratory Automation*,
635   *20*(3), 216–250. https://doi.org/10.1177/2211068214566939

636   27. Trappmann, B., Baker, B. M., Polacheck, W. J., Choi, C. K., Burdick, J. A., & Chen, C. S.
637   (2017). Matrix degradability controls multicellularity of 3D cell migration. *Nature*
638   *Communications*, *8*(1), 371. https://doi.org/10.1038/s41467-017-00418-6

639   28. Nguyen, D.-H. T., Lee, E., Alimperti, S., Norgard, R. J., Wong, A., Lee, J. J.-K., Eyckmans,
640   J., Stanger, B. Z., & Chen, C. S. (2019). A biomimetic pancreatic cancer on-chip reveals
641   endothelial ablation via ALK7 signaling. *Science Advances*, *5*(8), eaav6789.
642   https://doi.org/10.1126/sciadv.aav6789

643   29. Guan, Y., Xu, D., Garfin, P. M., Ehmer, U., Hurwitz, M., enns, G., Michie, S., Wu, M.,
644   Zheng, M., Nishimura, T., Sage, J., & Peltz, G. (2017). Human hepatic organoids for the
645   analysis of human genetic diseases. *JCI Insight*, *2*(17).
646   https://doi.org/10.1172/jci.insight.94954

647   30. Sampaziotis, F., Brito, M. C. de, Madrigal, P., Bertero, A., Saeb-Parsy, K., Soares, F. A. C.,
648   Schrumpf, E., Melum, E., Karlsen, T. H., Bradley, J. A., Gelson, W. T. H., Davies, S., Baker,
649   A., Kaser, A., Alexander, G. J., Hannan, N. R. F., & Vallier, L. (2015). Cholangiocytes
650   derived from human induced pluripotent stem cells for disease modeling and drug validation.
651   *Nature Biotechnology*, *33*(8), 845–852. https://doi.org/10.1038/nbt.3275

652   31. Ogawa, M., Ogawa, S., Bear, C. E., Ahmadi, S., Chin, S., Li, B., Grompe, M., Keller, G.,
653   Kamath, B. M., & Ghanekar, A. (2015). Directed differentiation of cholangiocytes from
654   human pluripotent stem cells. *Nature Biotechnology*, *33*(8), 853–861.
655   https://doi.org/10.1038/nbt.3294

656   32. Glaser, S. S., Gaudio, E., Rao, A., Pierce, L. M., Onori, P., Franchitto, A., Francis, H. L.,
657   Dostal, D. E., Venter, J. K., DeMorrow, S., Mancinelli, R., Carpino, G., Alvaro, D., Kopriva,
658   S. E., Savage, J. M., & Alpini, G. D. (2009). Morphological and functional heterogeneity of
659   the mouse intrahepatic biliary epithelium. *Laboratory Investigation*, *89*(4), 456–469.
660   https://doi.org/10.1038/labinvest.2009.6

661   33. Tian, G., Sobotka-Briner, C. D., Zysk, J., Liu, X., Birr, C., Sylvester, M. A., Edwards, P. D.,
662   Scott, C. D., & Greenberg, B. D. (2002). Linear Non-competitive Inhibition of Solubilized
663   Human γ-Secretase by Pepstatin A Methylester, L685458, Sulfonamides, and
664   Benzodiazepines. *Journal of Biological Chemistry*, *277*(35), 31499–31505.
665   https://doi.org/10.1074/jbc.m112328200

666   34. Alimperti, S., Mirabella, T., Bajaj, V., Polacheck, W., Pirone, D. M., Duffield, J., Eyckmans,
667   J., Assoian, R. K., & Chen, C. S. (2017). Three-dimensional biomimetic vascular model
668   reveals a RhoA, Rac1, and N-cadherin balance in mural cell–endothelial cell-regulated barrier
669   function. *Proceedings of the National Academy of Sciences*, *114*(33), 8758–8763.
670   https://doi.org/10.1073/pnas.1618333114

671   35. Bhatia, S. N., Underhill, G. H., Zaret, K. S., & Fox, I. J. (2014). Cell and tissue engineering
672   for liver disease. *Science Translational Medicine*, *6*(245), 245sr2-245sr2.
673   https://doi.org/10.1126/scitranslmed.3005975

674   36. Stevens, K. R., Scull, M. A., Ramanan, V., Fortin, C. L., Chaturvedi, R. R., Knouse, K. A.,
675   Xiao, J. W., Fung, C., Mirabella, T., Chen, A. X., McCue, M. G., Yang, M. T., Fleming, H.
676   E., Chung, K., Jong, Y. P. de, Chen, C. S., Rice, C. M., & Bhatia, S. N. (2017). In situ
677   expansion of engineered human liver tissue in a mouse model of chronic liver disease.
678   *Science Translational Medicine*, *9*(399), eaah5505.
679   https://doi.org/10.1126/scitranslmed.aah5505

680   37. Zong, Y., Panikkar, A., Xu, J., Antoniou, A., Raynaud, P., Lemaigre, F., & Stanger, B. Z.
681   (2009). Notch signaling controls liver development by regulating biliary differentiation.
682   *Development*, *136*(10), 1727–1739. https://doi.org/10.1242/dev.029140

683   38. Hofmann, J. J., Zovein, A. C., Koh, H., Radtke, F., Weinmaster, G., & Iruela-Arispe, M. L.
684   (2010). Jagged1 in the portal vein mesenchyme regulates intrahepatic bile duct development:
685   insights into Alagille syndrome. *Development*, *137*(23), 4061–4072.
686   https://doi.org/10.1242/dev.052118

687   39. Kitade, M., Factor, V. M., Andersen, J. B., Tomokuni, A., Kaji, K., Akita, H., Holczbauer,
688   A., Seo, D., Marquardt, J. U., Conner, E. A., Lee, S.-B., Lee, Y.-H., & Thorgeirsson, S. S.
689   (2013). Specific fate decisions in adult hepatic progenitor cells driven by MET and EGFR
690   signaling. *Genes & Development*, *27*(15), 1706–1717.
691   https://doi.org/10.1101/gad.214601.113

692   40. MICHALOPOULOS, G. K., BOWEN, W. C., MULÈ, K., & LUO, J. (2003). HGF-, EGF-,
693   and Dexamethasone-Induced Gene Expression Patterns During Formation of Tissue in
694   Hepatic Organoid Cultures. *Gene Expression*, *11*(2), 55–75.
695   https://doi.org/10.3727/000000003108748964

696   41. Totaro, A., Castellan, M., Battilana, G., Zanconato, F., Azzolin, L., Giulitti, S., Cordenonsi,
697   M., & Piccolo, S. (2017). YAP/TAZ link cell mechanics to Notch signalling to control
698   epidermal stem cell fate. *Nature Communications*, *8*(1), 15206.
699   https://doi.org/10.1038/ncomms15206

700   42. Kaylan, K. B., Berg, I. C., Biehl, M. J., Brougham-Cook, A., Jain, I., Jamil, S. M., Sargeant,
701   L. H., Cornell, N. J., Raetzman, L. T., & Underhill, G. H. (2018). Spatial patterning of liver
702   progenitor cell differentiation mediated by cellular contractility and Notch signaling. *ELife*, *7*,
703   e38536. https://doi.org/10.7554/elife.38536

704   43. Rimland, C. A., Tilson, S. G., Morell, C. M., Tomaz, R. A., Lu, W., Adams, S. E.,
705   Georgakopoulos, N., Otaizo-Carrasquero, F., Myers, T. G., Ferdinand, J. R., Gieseck, R. L.,
706   Sampaziotis, F., Tysoe, O. C., Wesley, B., Muraro, D., Oniscu, G. C., Hannan, N. R., Forbes,
707   S. J., Saeb-Parsy, K., … Vallier, L. (2020). Regional differences in human biliary tissues and
708   corresponding in vitro derived organoids. *Hepatology*. https://doi.org/10.1002/hep.31252

709   44. Mehta, G., Williams, C. M., Alvarez, L., Lesniewski, M., Kamm, R. D., & Griffith, L. G.
710   (2010). Synergistic effects of tethered growth factors and adhesion ligands on DNA synthesis

711   and function of primary hepatocytes cultured on soft synthetic hydrogels. *Biomaterials*,

712   *31*(17), 4657–4671. https://doi.org/10.1016/j.biomaterials.2010.01.138
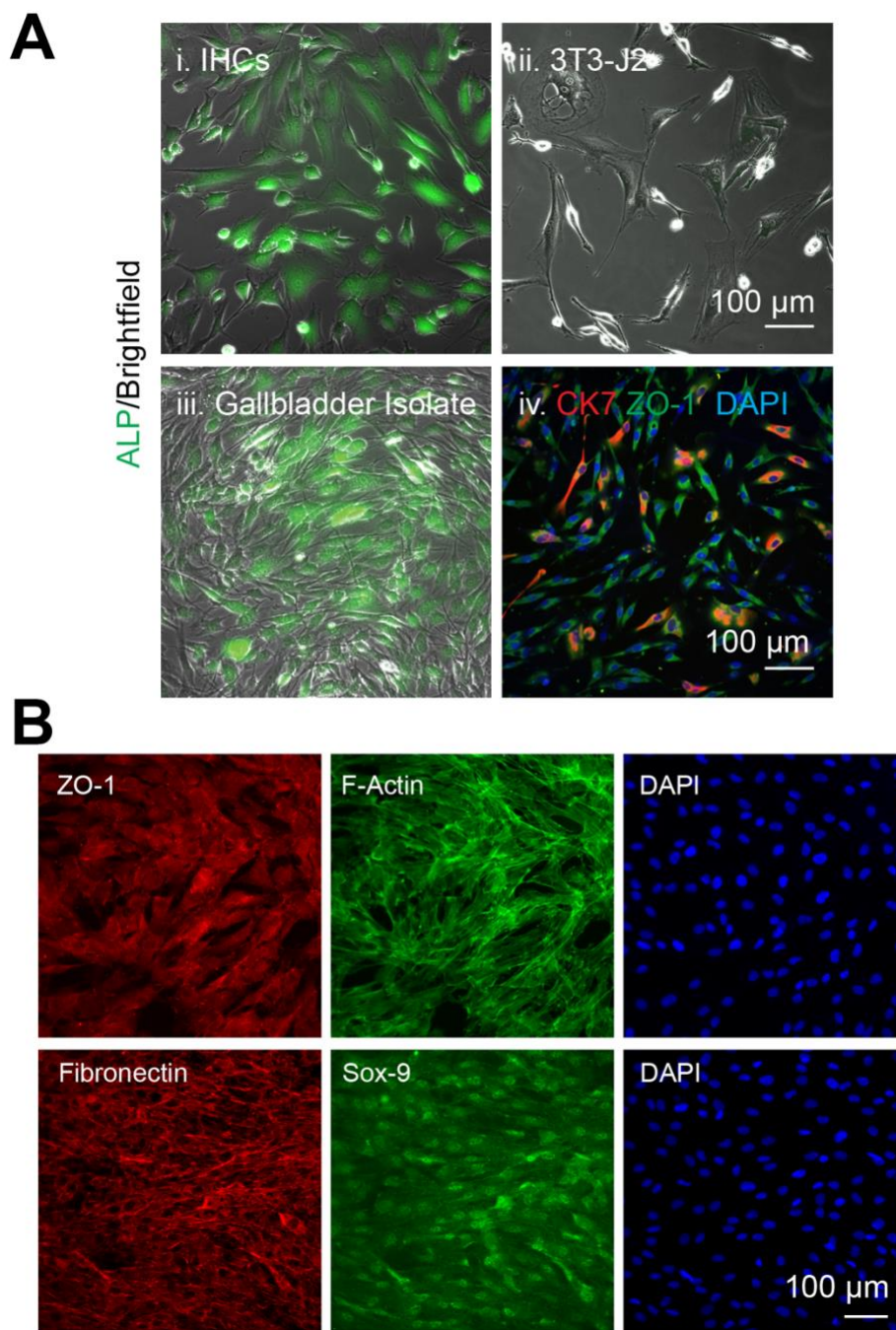
713

714

715

716

717 **SUPPLEMENTAL FIGURES**

718

719 **Supplementary Figure 1. Characterization of Cholangiocyte Populations.** (A)
720 Alkaline phosphatase (ALP) uptake comparison between (i) intrahepatic cholangiocytes
721 (IHCs), (ii) control J2-3T3 mouse fibroblasts and (iii) fresh extrahepatic cholangiocyte
722 (EHCs) isolates from human gallbladder tissue. (iv) Immunofluorescence staining of fresh
723 EHCs.
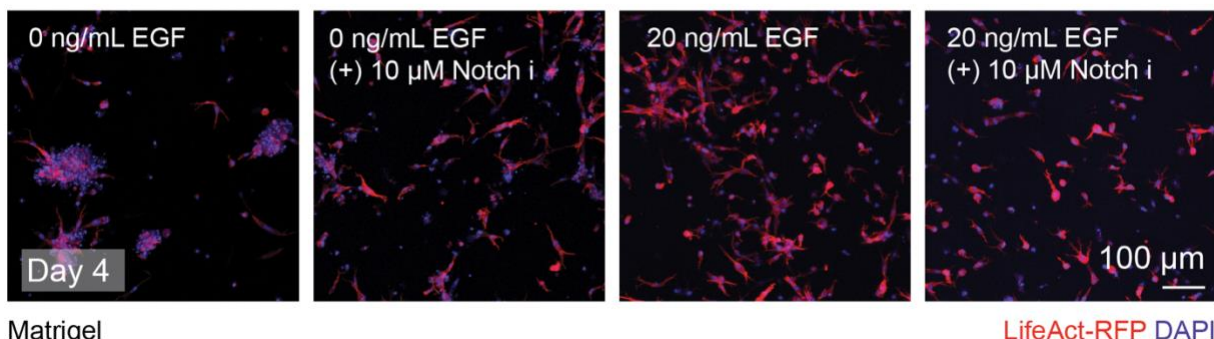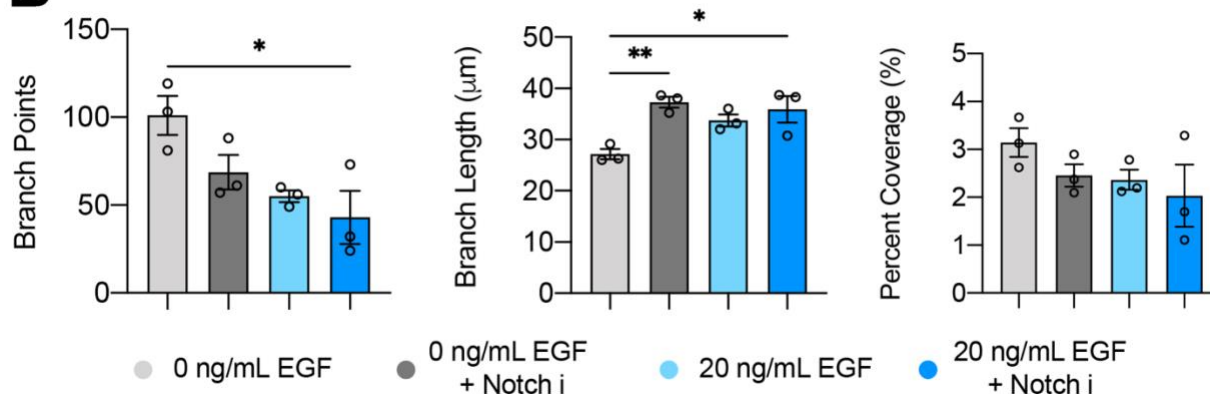
Supplemental Figure 2. 3D Culture in Matrigel Does Not Support Cholangiocyte Branching Morphogenesis. **(A)** Representative images of LifeAct RFP-IHCs encapsulated in Matrigel, cultured with and without EGF or Notch inhibition (10 μM L,685,458). **(B)** Quantification of branch length, points, and network percent coverage. Image data were generated from at least 3 independent fields of view from 3 biological replicate experiments. P-values were obtained by a One-Way ANOVA Tukey's hypothesis test. P < 0.033 (*), P< 0.002 (**), P <0.001 (***). All data represented as mean ± SEM.
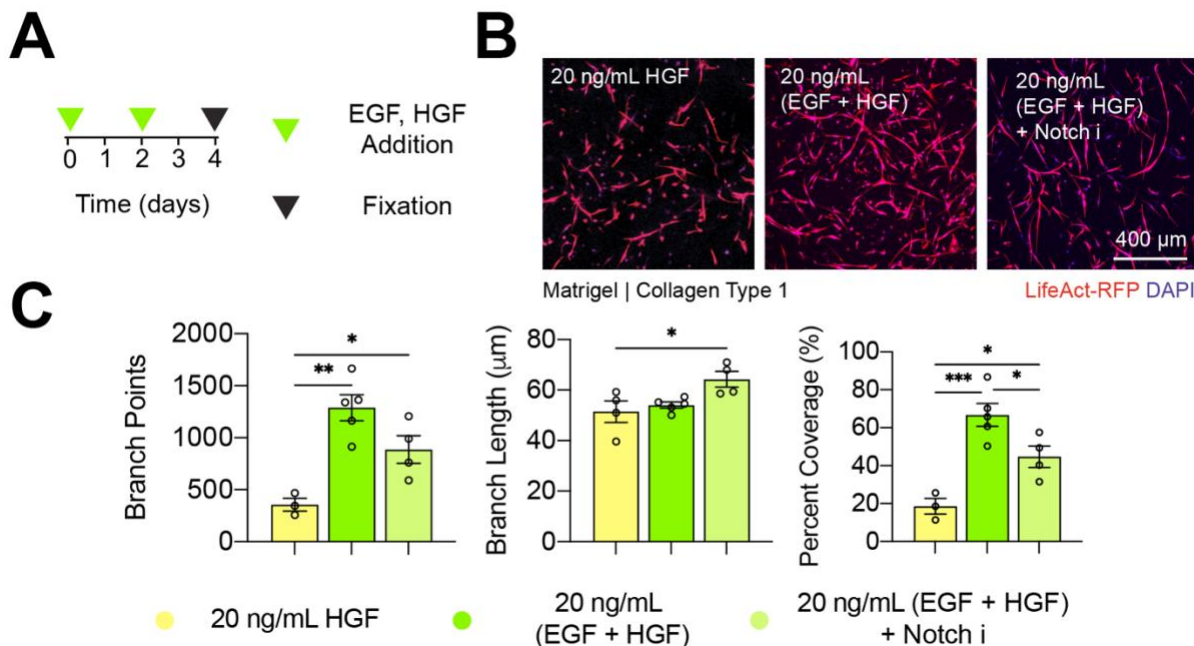
Supplemental Figure 3. Hepatocyte Growth Factor (HGF) Supplementation Enhances Cholangiocyte Branching in Matrigel/Collagen Type 1 Hydrogel Blends. (A) Experimental approach to test the roles of HGF supplementation on IHC-RFP branching. (B) Representative maximum intensity projection of z-stack confocal images taken four days post encapsulation. (C) Quantification of percent coverage, major and minor axis length from at least 3 different fields of view from biological replicate experiments (n =3). P-values were obtained by a One-Way ANOVA Tukey's hypothesis test. $P < 0.033$ (*), $P < 0.002$ (**), $P < 0.001$ (***). All data represented as mean ± SEM.

31
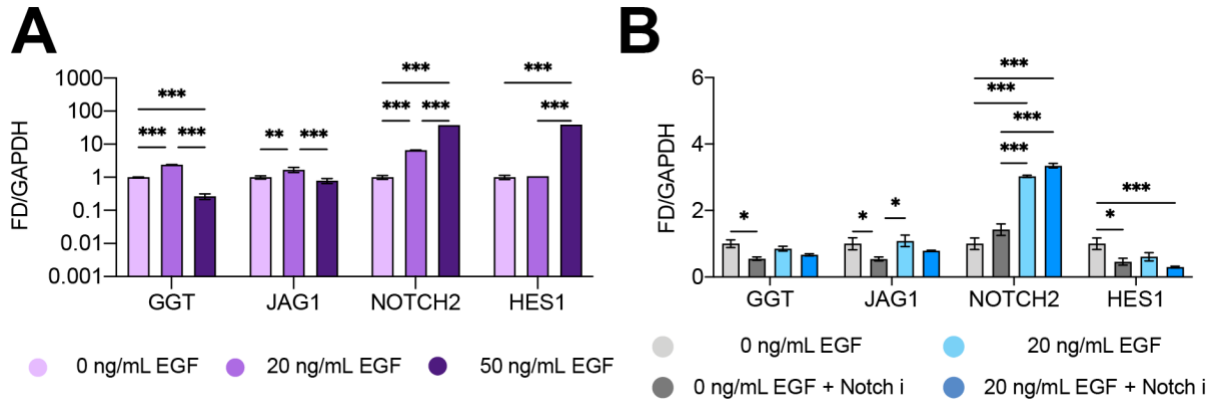
Supplemental Figure 4. Effects of EGF Stimulation on Notch Signaling in 2D. (A) mRNA expression of *GGT*, *JAG1*, *NOTCH2* and *HES1* of IHCs cultured in the same dose regiment as 3D cultures (media exchanged every two days) with 0, 20 and 50 ng/mL EGF stimulation. Data is shown from pooled independent 2D cultures (n = 3 biological replicates). (B) mRNA expression of the aforementioned genes, of IHCs cultured in 2D, under 0 and 20 ng/mL EGF stimulation with and without Notch inhibition. Cells were harvested after 4 days following media exchanges every two days. P-values were obtained via Two-Way ANOVA Tukey's hypothesis testing. $P < 0.033$ (*), $P < 0.002$ (**), $P < 0.001$ (***). All data represented as mean ± SEM.
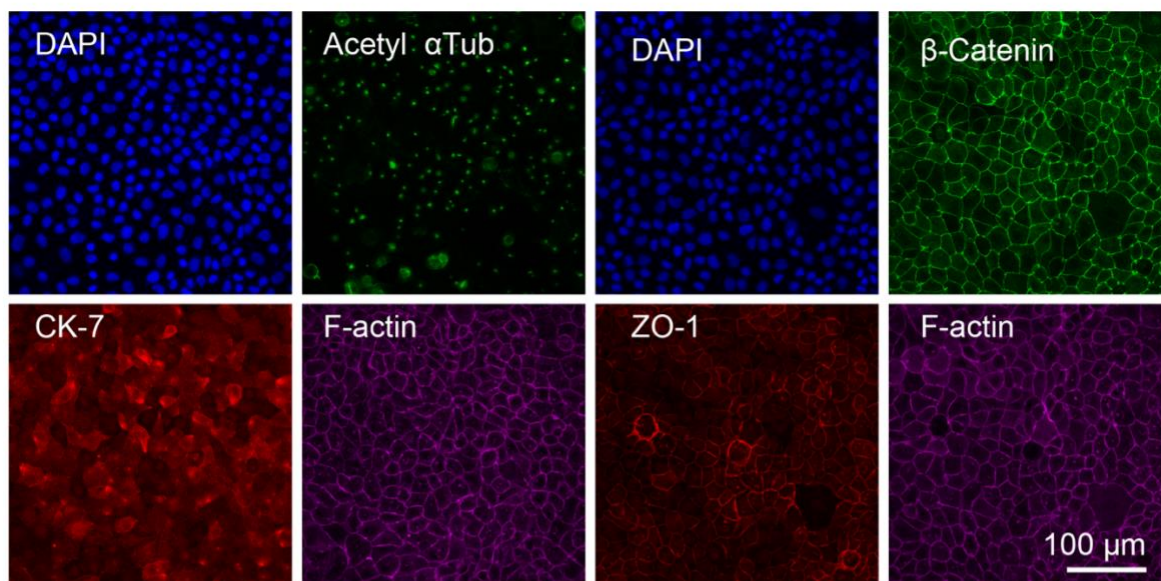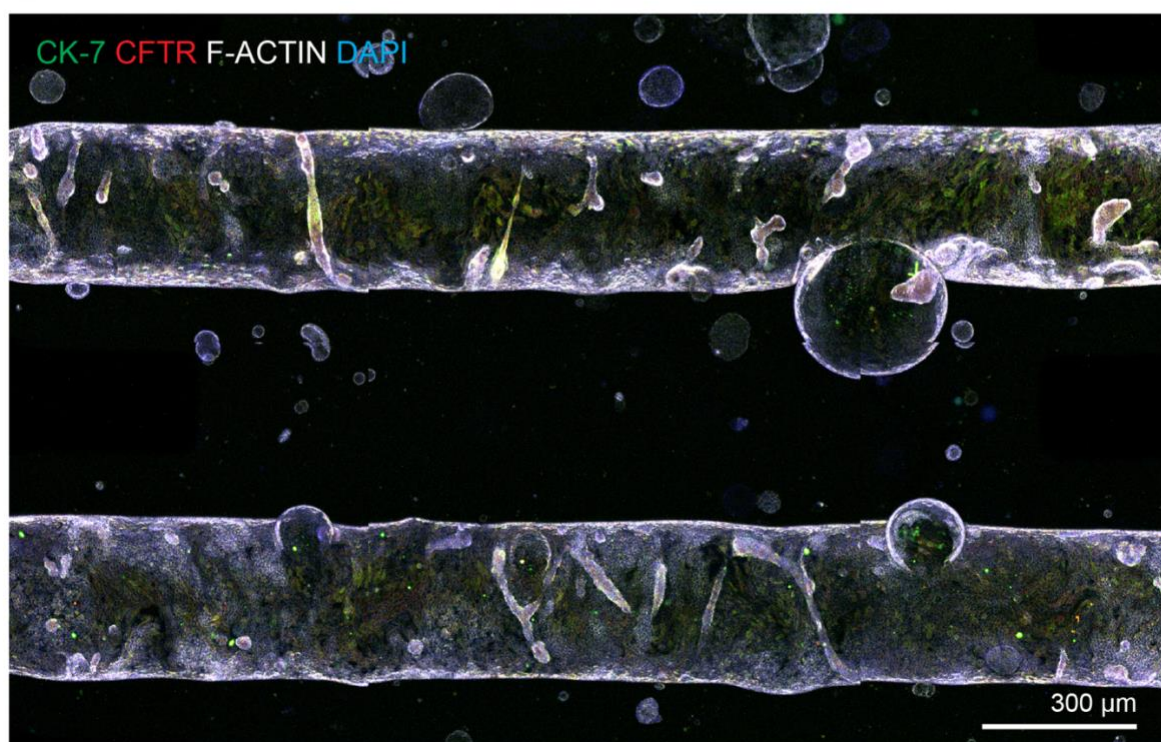
Supplementary Figure 5: Microfluidic Culture of Normal Rat Cholangiocytes. (A) Immunofluorescence stains of normal rat cholangiocytes (NRCs) cultured in 2D for biliary (CK-7), primary cilia (acetylated α-tubulin; Acetyl αTub) and junctional markers (ZO-1 and β-catenin). (B) Microfluidic culture of NRCs in the dual microfluidic device.

784 **Supplementary Table 1: Primary and Secondary Antibodies**
785 **Supplementary Table 2: Reagents Used**
786 **Supplementary Table 3: q-RT PCR Primer List**
787
788 **Table S1: Antibodies**

Primary Antibodies	Source	Cat no	Host Species	Dilution
Cytokeratin-19	Abcam	ab7754	Mouse	1:200
Cytokeratin-7	Abcam	ab181598	Rabbit	1:100
CFTR	Abcam	ab2784	Mouse	1:200
Fibronectin	Abcam	ab2413	Rabbit	1:250
ZO-1	Invitrogen	40-2200	Rabbit	1:100
β-catenin	Cell Signaling	L54E2 (2677S)	Mouse	1:5
HNF-1β	Santa Cruz Biotechnology	sc-130407	Mouse	1:200
SOX9	Santa Cruz Biotechnology	sc-166505	Mouse	1:200
Alexa Fluor 546	Life Technologies (Eugene, OR)	A11010	Goat anti-rabbit	1:500
Alexa Fluor 546	Life Technologies	A11003	Goat anti-mouse	1:500
Alexa Fluor 488	Life Technologies	A21206	Donkey anti-rabbit	1:500
Alexa Fluor 647	Life Technologies	A22287	Phalloidin	1:1000
Cytokeratin 7 Antibody (RCK105) PE	Santa Cruz Biotechnology	sc-23876 PE	Human	1:200
AFP Antibody (C3) Alexa Fluor® 647	Santa Cruz Biotechnology	sc-8399 AF647	Human	1:200
Anti-alpha 1 Antitrypsin antibody [EPR9090] (Alexa Fluor® 647)	Abcam	ab206735	Human	1:200
PE Mouse Anti-Human IgG	BD Biosciences	555787	Human	1:200
Alexa Fluor® 647 Mouse IgG1 κ Isotype Control	BD Biosciences	557714		1:200
DAPI	ThermoFisher	D1306		1:50,000

789
790
791

34

792 **Table S3: Reagents**

Chemicals, Peptides and Recombinant Proteins	Source	Cat No.
Alkaline Phosphatase Live Stain	Life Technologies	A14353
Rhodamine 123 (100 μM)	Sigma-Aldrich	83702-10MG
γ-Glutamyl Transferase (GGT) Activity Fluorometric Assay Kit	Sigma-Aldrich	MAK090-1KT
Recombinant Human EGF	R&D	236-EG-200
L-685,458 (Notch Inhibitor)	Tocris Biosciences	2627
rLV-Ubi-LifeAct TagRFP Lentiviral Vectors	Ibidi	60142

793
794 **Table S2: Primer Set**

Primers	Source	Assay ID
GGT	Life Technologies	Hs00980756_m1 FAM
JAGGED1	Life Technologies	Hs01070032_m1 FAM
NOTCH2	Life Technologies	Hs01050702_m1 FAM
HES1	Life Technologies	Hs00172878_m1 FAM

795
796
797